Results in Engineering 22 (2024) 102166

Contents lists available at ScienceDirect

Results in Engineering

journal homepage: www.sciencedirect.com/journal/results-in-engineering

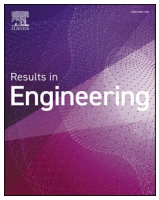

Erosion behaviour of cold sprayed stainless-steel coatings for civil infrastructures: An energetic approach

Rocío Cortés [a,*], Miguel Ángel Garrido-Maneiro [a], Pedro Poza [a,b]

[a] DIMME – Durability and Mechanical Integrity of Structural Materials, Escuela Superior de Ciencias Experimentales y Tecnología, Universidad Rey Juan Carlos, c/ Tulipán s/n, 28933, Móstoles, Madrid, Spain
[b] ITPS – Institute of Technologies for Sustainability, Universidad Rey Juan Carlos, c/Tulipán s/n, 28933, Móstoles, Madrid, Spain

ARTICLE INFO

Keywords:
Cold spray
Stainless steel
Coating
Erosion
Stress-strain curves
Indentation
Civil infrastructures

ABSTRACT

Along with corrosion, erosion is one of the main causes of damage to civil infrastructures. The continuous impact of fine particles carried by the air produces a deterioration in the elements of these structures. When this damage is significant, these elements are replaced by new ones. In this work, the possibility of extending the useful life of these components by spraying coatings on the damaged areas is proposed. In this sense, repair techniques such as cold spray deposition are possibilities for this purpose. Therefore, this study focuses on evaluating the erosion behaviour of stainless-steel coatings deposited on structural steel. In addition, the erosion results have been correlated with the model proposed by Hutchings, and an energetic interpretation of the erosion process through this model has been proposed. To carry out this study, stainless steel coatings have been deposited on carbon steel substrates to improve their resistance to corrosion. Different spraying temperatures, from 800 °C to 1100 °C, combined with different pressures of the carrier gas, from 40 to 70 bar, have been analysed. The elastic moduli of the coatings, and their stress-strain curve, have been determined by depth sensing indentation tests with Berkovich and spherical tips, respectively. Erosion tests with normal incidence have been programmed to obtain the corresponding erosion rates. From the results of this work, the optimal projection conditions of stainless steel on carbon steel substrates for the repair of civil infrastructures subjected to erosion processes could be identified.

1. Introduction

Cold spray (CS) is a thermal deposition technique in which metallic materials and alloys are deposited on substrates. In CS, the powder material is accelerated in a gas stream through a convergent-divergent nozzle at temperatures below the melting point of the sprayed material and at speeds up to two or three times the speed of sound (i.e., 500 m/s or 1200 m/s) [1–3].

Since the particles are sprayed at a temperature below the melting point, CS is categorized as a solid-state deposition method in which the coating build-up mechanism occurs by plastic deformation. Therefore, CS minimizes or eliminates phenomena that are detrimental in conventional thermal spraying techniques, where the spraying temperatures reach the melting point of the material, such as thermally induced residual stresses, melting, oxidation, phase transformation, decomposition, and grain growth [4]. Due to the fact that the adhesion process between sprayed particles and the substrate requires a high plastic deformation, it is necessary that the particle velocity should exceed a certain threshold value, the so-called critical impact velocity [2,5–8]. This velocity is dependent on the particle and substrate material properties [9,10], as well as spraying conditions such as gas temperature, pressure and type, particles size, stand-off distance to the substrate, and geometry of the nozzle [2,11–13].

In general, the temperature and pressure of the gas have a decisive impact on the coating quality. Shabani Chafjiri et al. [14] deposited copper and alumina copper on an AZ31 alloy at different combinations of pressures and stand-off distance. They observed that increasing the pressure (10–30 bar) and decreasing the stand-off distance (3 cm–1 cm) leads to a decrease in porosity, achieving more dense coatings. Regarding an increase in temperature, Villa et al. [15] have shown that it contributes to this the compaction process. These authors deposited 316L stainless steel (SS) powder onto an aluminium alloy substrate at different combinations of temperatures and pressures. The quality and deposition efficiency of the coating increased with increasing pressure and temperature.

For the coatings to perform their repair function effectively, it is a

* Corresponding author.
E-mail addresses: rocio.cortes@urjc.es (R. Cortés), miguelangel.garrido@urjc.es (M.Á. Garrido-Maneiro), pedro.poza@urjc.es (P. Poza).

https://doi.org/10.1016/j.rineng.2024.102166
Received 19 January 2024; Received in revised form 21 March 2024; Accepted 19 April 2024
Available online 28 April 2024

necessary condition that their properties be similar or improved with respect to the material they repair. One of the applications where damage is continuous is civil infrastructures, most of them made of which carbon steel. Low-carbon steel provides an eco-friendly solution for construction and structural applications. It is widely employed in the construction, petroleum, mining, hydropower, maritime, automotive, and chemical industries [16–18]. However, there are limits to the durability of carbon steel because of its low corrosion and erosion resistance. Carbon steel tubing and piping are susceptible to erosion–corrosion damage due to the erosive and corrosive nature of the produced fluid or gas [19]. A similar damage is the one suffered by the structural elements of civil infrastructures such as railway bridges, where the impact of fine particles transported by the wind and the effect of humidity generate a process of erosion combined with corrosion [20]. To identify these defects, regular assessments are carried out. These are intended to determine the replacement of damaged elements, although this generates a lot of waste. Therefore, the possibility of repairing these damaged areas rather than replacing them with new ones is considered. This generates a reduction in waste, creating a more sustainable infrastructure [21].

In this work, the possibility of using the CS technique to deposit coatings on the damaged areas of these carbon steel components is considered. The viability of CS for this purpose, requires that the manufactured coating has, at least, the same behaviour and properties as the material it repairs, that is, the deposited coating must be resistant to both erosion and corrosion. This last condition can be guaranteed by depositing austenitic stainless steel on the carbon steel material.

There are previous studies in which the erosion behaviour of carbon steel and austenitic stainless steel were analysed. Islam et al. [22] analysed the effect of microstructure on erosion behaviour of carbon steel used for oil and gas pipes. In that study, sets of erosion experiments were carried out on AISI 1018 and AISI 1080 steels at different impingement angles to identify the effect of microstructure on erosion and to investigate the degradation mechanisms. They concluded that the erosion rates of both steels increased with increasing particle velocity and decreased with increasing impact angle. Additionally, they reported that at low impact angle, ploughing, and cutting were the dominant erosion mechanism. However, at high impact angle, flattening of ridges, and fracture were the dominant process of metal removal.

Other research on the solid particle erosion behaviour of stainless steel 201, 304, 316, and 420 was carried out by Chowdhury et al. [23]. In this work, the erosion tests were based on ASTM G-32. They analysed the influence of different velocities (40–60 m/s) and impingement angles (15–90°) on the erosion rates. With respect to abrasive particles, they used silica sand, aluminium oxide, and ferric oxide, with particle sizes smaller than 150 μm and 150–300 μm. They noted that all steels had a maximum erosion rate at a 60° impingement angle. Analysing the erosion tracks by scanning electron microscopy, plastic deformation was identified as the dominant mechanism. Consequently, all steels presented ductile behaviour during the erosion process.

Currently there are different analytical models that relate the erosion wear rate with material properties. One of the most used is the model proposed by Hutchings [24]. This author presented a theoretical analysis for the erosion of metals by spheres at normal incidence. This model uses a criterion based on the critical plastic strain. That is, when the material reaches a threshold value of plastic deformation, the erosion phenomenon occurs. According to this model, the erosion rate, $T_{erosion}$, is given by the following equation [24]:

$$T_{erosion} = K_D \frac{\rho\, \sigma^{1/2} v^3}{\varepsilon_c^2\, H^{3/2}} \tag{1}$$

where ρ is the target material density, σ is the eroding particles' density, H is the indentation hardness of the metal target, and ε_c represents the critical strain. The K_D coefficient refers to the fraction of material removed with respect to the indentation volume, that is, this parameter describes the severity of the erosion process. The hardness of the metal may be calculated from measurements of indentations, but the critical strain is not readily measured and must be derived from experimental measurements of the erosion rate. Hussain et al. [25] determined the critical strain at normal impingement angle for different velocities from experimental erosion tests carried out onto ferritic stainless steels, austenitic stainless steel, and low carbon steel. However, its determination requires assuming a certain value for the fraction of the volume of the indentation that is removed during the erosion process. These authors considered a value of 1 for this fraction. Therefore, the evaluation of the erosion process severity through this model is not straightforward.

Therefore, to consider the possibility of implementing this repair technique, it is necessary to know the erosion resistance of the coatings obtained by CS. In this way, the optimal spraying conditions for repairing damaged components by erosion could be identified. However, there are not many works where the erosion behaviour of steel coatings deposited by the cold spray technique is studied. Singh et al. [26] performed a comparative erosion wear study of uncoated, high velocity oxy-fuel (HVOF)-coated, and CS-coated samples of T-91 steel. They programmed erosion tests at 800 °C for different impingement angles. They observed that the maximum weight loss of samples during the erosive process was at a 30° impingement angle and a 2 g/min flow rate. Additionally, they reported that the cold sprayed coatings showed the highest wear resistance. Unfortunately, we have not found recent publications on the study of erosion of stainless-steel coatings deposited by the cold spray technique. This circumstance has been the driving force for this research.

In this work, the behaviour against erosion of 316L stainless steel coatings deposited on a low carbon S355J2 steel by the cold spray technique was analysed. For this, coatings were deposited under different spraying conditions. A morphological and microstructural characterisation was performed on each coating to estimate the thickness and porosity in previous research [27]. Erosion tests were carried out at room temperature and the erosion rates for each coating were estimated. To correlate the erosion behaviour of the coatings with their mechanical properties, instrumented indentation tests were performed with a spherical indenter and the corresponding stress-strain curves were obtained. From these curves, an energetic model was proposed to estimate the severity of the erosion process of the coatings.

2. Material and methods

Stainless steel 316L powders with a particle size of −50 + 15 μm were sprayed onto low carbon S355J2 steel by CS with Plasma Giken PCS 1000 equipment (Saitama, Japan). The coatings were sprayed under different pressures, 40–70 bar, and temperatures, 800 °C to 1100 °C, using nitrogen as the propellant gas. The deposition was performed at Thermal Spray Centre in Barcelona (Spain). The rest of the spraying parameters can be consulted in previous reports [27,28]. Table 1 detailed the CS temperatures and pressures values.

Morphological characterisation was carried out by optical microscopy (Motic BA310 Met-T, Xiamen, China) and scanning electron microscopy (SEM) (Hitachi S3400 N, Tokyo, Japan) in order to evaluate the coatings' thickness and porosity. Cross sections of the different coatings were obtained by a cutting process with an alumina wheel (Isomet 5000 Buehler). Subsequently, a metallographic procedure was carried out according to the ASTM E3-95 standard. Therefore, these samples were embedded in a low stiffness resin and, afterwards, were roughed with SiC papers and polished with a diamond suspension up to 1 μm. A total of 10 images were taken along each coating with a Moticam 3.0 MP digital camera. The thickness and porosity values were obtained using image analysis software (Motic Images Advanced 3.2).

Nanoindentation tests (matrix of 10x5 on each coating) were programmed to determine the elastic modulus (E) and hardnesses (H) of the 316L coating and S355J2 substrate using a Nanoindenter G200 equipment (Agilent, USA). The continuous stiffness measurement (CSM)

Table 1
Temperatures and pressures values for the CS process.

CS conditions		
Temperature (°C)	Gas pressure (bar)	Sample
800	*40*	CS_800_40
	50	CS_800_50
	60	CS_800_60
	70	CS_800_70
900	*40*	CS_900_40
	50	CS_900_50
	60	CS_900_60
	70	CS_900_70
1000	*40*	CS_1000_40
	50	CS_1000_50
	60	CS_1000_60
	70	CS_1000_70
1100	*50*	CS_1100_50
	60	CS_1100_60
	70	CS_1100_70

methodology was selected and a Berkovich tip with a tip radius of 20 nm was used. During the indentation tests, multiple loading-unloading cycles of 2 nm of displacement were superimposed on the main loading process with a frequency of 35 Hz up to 1000 nm of total penetration depth [27]. The values of both properties were obtained for each cycle according to the Oliver-Phar methodology [29]. Therefore, an evolution of E and H with the penetration depth could be obtained during the main indentation cycle. Additionally, another batch of nanoindentation tests were carried out by mounting spherical tips with two different radii, 5 μm and 500 μm. The purpose of these tests was to obtain the indentation stress-strain curves of the coatings using the same CSM methodology previously described and the equations proposed by Pathak et al. [30]. This methodology allows extracting evolution of the force, P, displacement of the indenter, h_t, and the contact stiffness, S, between indenter and indented surface. Combining these data with the equations proposed by Pathak et al., it was possible to obtain the corresponding indentation stress-strain curves for each coating. The indentation stress, σ_{ind} and indentation strain, ε_{ind}, were defined through the following equations [30,31].

$$\sigma_{ind} = \frac{P}{A_c} = \frac{P}{\pi\, a^2} \tag{2}$$

where A_c is the contact area and a is the contact radius:

$$\varepsilon_{ind} = \frac{h_t}{2.4\, a} \tag{3}$$

The contact radius, a, can be estimated through the contact stiffness, S, according to the following equation [32]:

$$a = \frac{S}{2 \bullet E^*} \tag{4}$$

where E* represents the effective modulus define according to Equation (5):

$$\frac{1}{E^*} = \frac{1-\upsilon^2}{E} + \frac{1-\upsilon_i^2}{E_i} \tag{5}$$

E* considers that the elastic displacements occur both in the indenter and in the material and depends on the tip indenter's properties (terms with the sub-index *i*) and those of the material (terms without a sub-index). In this work, diamond indenters were used, hence the Poisson's ratio was 0.07 and the elastic modulus was 1140 GPa. The indentations carried out using the tip with the lower radius were used to capture the elastic response of the material. The tip with the higher radius was selected to obtain the plastic behaviour of the coating.

The erosion tests were programmed according to ASTM G76 requirements [33]. Multi-angular abrasive particles of alumina with an average size of 50 μm were used. A similar particle geometry has been previously selected by other authors [34]. The distance between the nozzle and coating was 10 mm. The abrasive particles were sprayed with a speed of 80 m/s and an impingement angle of 90° with regards to the target surface. These tests were performed at different times (10, 15, 20, 25, and 30 min). Before each erosion test, each sample was ultrasonically cleaned in an ethanol bath for 10 min. After that, they were dried in a furnace at 60 °C for 10 min. Finally, each sample was weighed in a balance. A similar procedure was followed on each sample after the erosion test. The erosion rates, $T_{erosion}$, were estimated using the difference in weight before and after the test, i.e., the material mass removed, and the mass of the incident particles, according to the following equation [35]:

$$T_{erosion} = \frac{Material\ mass\ removed}{mass\ of\ the\ incident\ particles} \tag{6}$$

The eroded samples were metallographically prepared following the same procedure as that described for morphological and microstructural characterization.

3. Results and discussions

Fig. 1 represents the thickness and porosity values measured on each coating. All coatings exhibited a thickness higher than 400 μm. The coatings deposited at a spraying temperature of 800 °C are the ones with the highest thickness. However, these coatings are the ones with the highest porosity. This makes this spraying condition not ideal for depositing 316L coatings. For spraying temperatures higher than this value, the thickness decreased significantly, with no relevant differences between 900 °C, 1000 °C, and 1100 °C; no significant effect from the pressure was observed. With respect to the porosity on each coating, the higher the spraying pressure, the lower the porosity. This tendency was observed for coatings deposited at 800 °C, 900 °C, and 1000 °C. However, no tendency was observed for the coating sprayed at 1100 °C. Additionally, the higher the spraying temperature, the lower the porosity. This tendency has also been previously reported by other authors [14,36–38]. The results shown in Fig. 1 were previously reported by Cortés et al. [27]. Knowing the value of the coatings' thickness is important to ensure that the material removed in the erosion tests is restricted to the coating material and that the substrate has never been eroded during these tests.

Fig. 2 shows representative SEM images of cross sections corresponding to CS_800_50 and CS_1100_50 coatings, representing two extreme spraying conditions within the range analysed in this work. Both images show the arrangement of splats in the respective deposits. Comparing both images, it can be observed that the splats corresponding to the CS_1100_50 coating show a larger capacity for deformation and conformation, being able to adapt to more complex geometries promoting a reduction of porosity or a lack of continuity between the splats. In addition, the internal structure of the splats also presents differences. CS_1100_50 coatings are characterised by having splats whose internal structure consists of elongated grains according to the direction of highest strain. This higher deformation capacity observed in the coatings deposited at 1100 °C compared to those deposited at 800 °C may be related to a decrease in the yield strength of the particles because of the increase in the spraying temperature [39]. This could explain the tendency observed in the porosity (Fig. 1). A higher temperature during deposition favours a better accommodation of the splats, avoiding porosity. Consequently, the plastic deformation accumulated in the coatings deposited at the highest temperature will be higher than that accumulated in the materials deposited at lower temperatures. The microstructure of the coatings deposited at 1100 °C is hardened by plastic deformation, like a work-hardened metal, reducing their deformation capability during service. Similar results were obtained by Shabani et al. [14].

Indentation tests were carried out on both the coatings and the substrates (S355J2 and SS316L). The aim of these tests is to obtain the

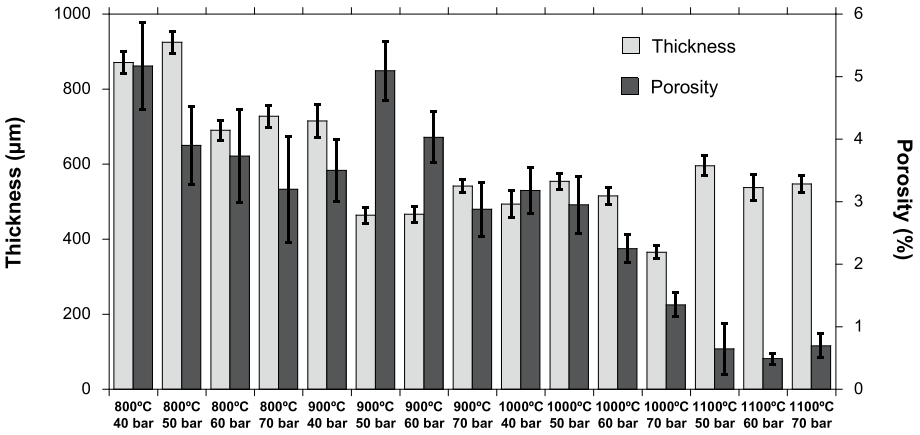

Fig. 1. Thickness and porosity values of the cold sprayed coatings.

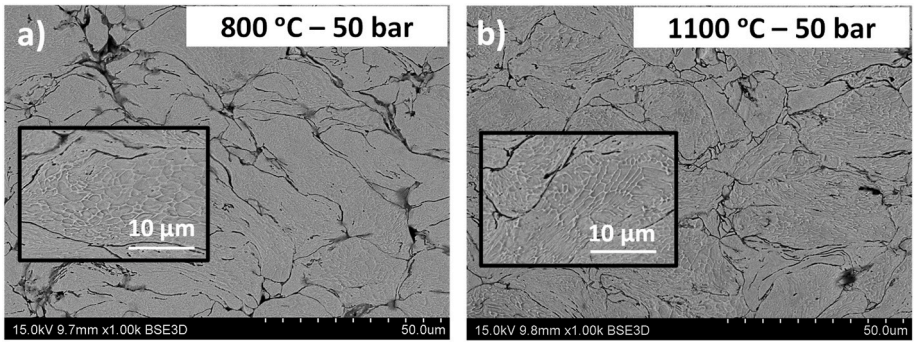

Fig. 2. SEM images of cross sections corresponding to cold sprayed coatings deposited at a) 800 °C – 50 bar (CS_800_50) and b) 1100 °C – 50 bar (CS_1100_50). A detailed image of the microstructure is also included, revealing the morphology within the splats.

elastic moduli. First, there must exist a linear relationship between contact stiffness and displacement into the surface for a homogeneous and isotropic material [32,40]. In this type of material, any loss of linearity may be due to the presence of defects such as porosity, cracks, or a lack of continuity. For this reason, it is necessary for this linear relationship to be present, ensuring that the results extracted from the indentation tests reflect the actual behaviour of the material. Fig. 3 a) shows two representative tests for the different substrates (S355J2 and SS316L). In both graphs, the substrates present a linear tendency.

Fig. 3 b) shows the elastic modulus evolution for SS316L and S355J2, applying the Oliver-Phar methodology on each cycle of the CSM record [29]. The elastic moduli remain constant in the interval from 200 to 1000 nm, according to the linear tendency shown in Fig. 3 a). Therefore, this range was used to obtain the average values for both materials, reporting values of 209 ± 7 GPa and 181 ± 9 GPa for S355J2 and SS316L, respectively.

The contact stiffness evolution with respect to displacement into the surface of a representative test for each coating is shown in Fig. 4. In most of the curves, a linear relationship was observed up to the maximum penetration depth. However, under some spraying

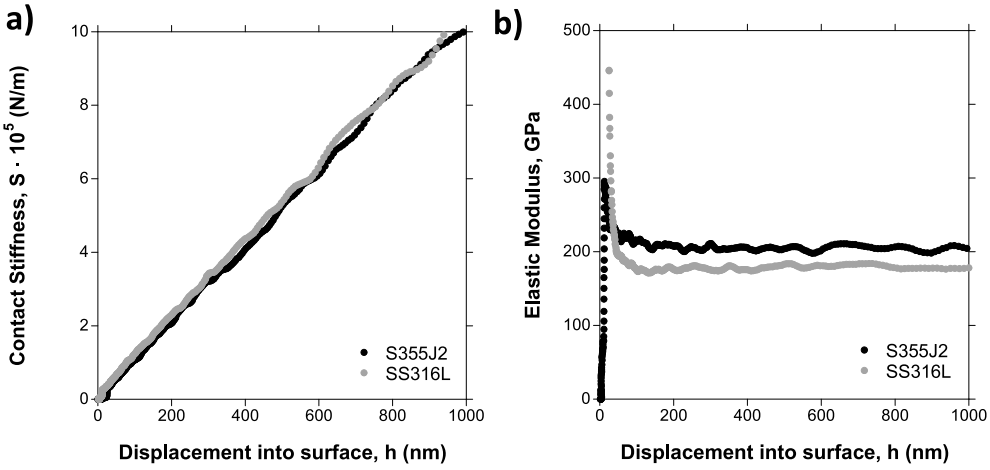

Fig. 3. a) Representative test for contact stiffness versus displacement into surface; b) Elastic modulus values versus displacement into surface for the substrate (SS316L) and substrate (S355J2).

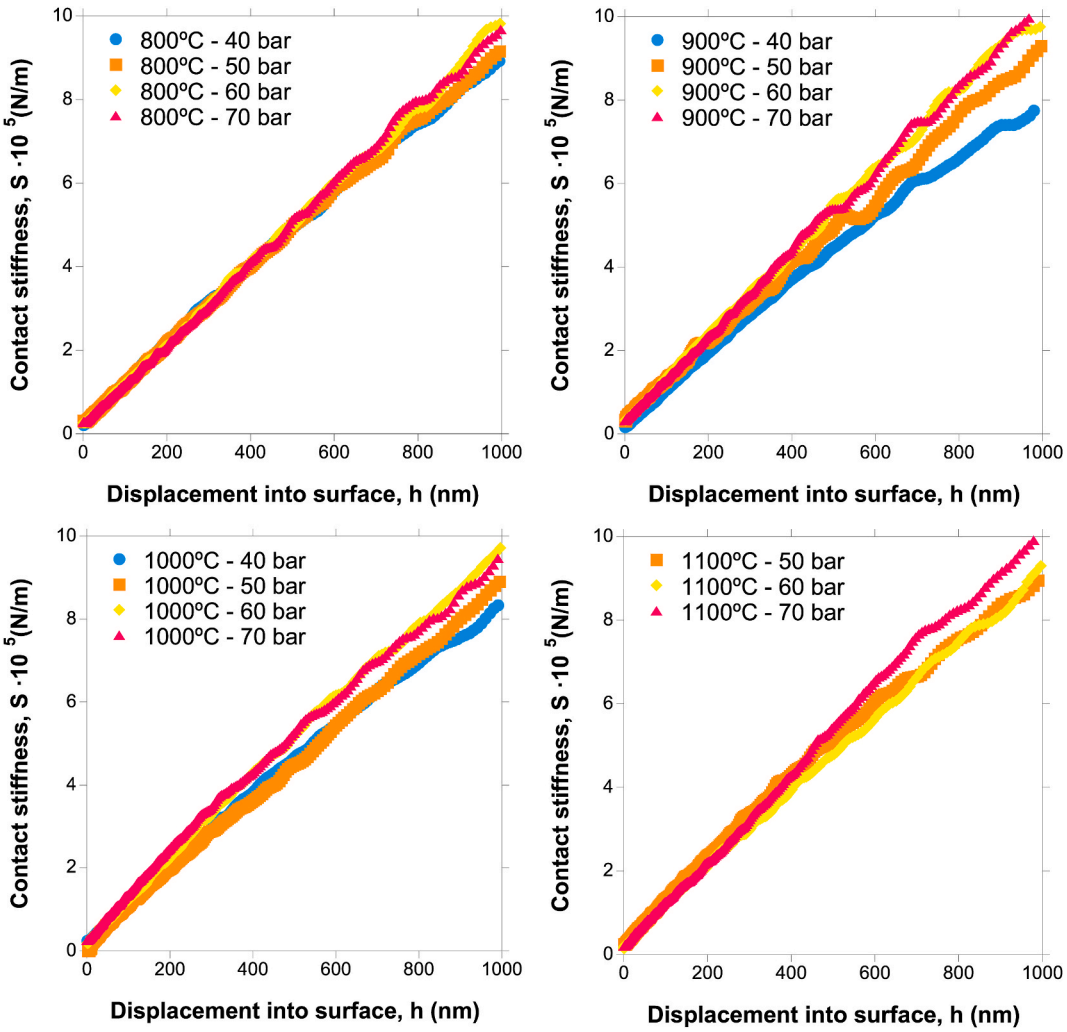

Fig. 4. Representative test for contact stiffness versus displacement into the surface under different spraying conditions.

conditions, a loss of linearity for contact stiffness occurs above a certain penetration depth. For coatings sprayed at 800 °C, a good linear fit for contact stiffness is observed for spray pressures of 50, 60, and 70 bar up to the maximum penetration depth of 1000 nm. However, for coatings sprayed at 40 bar, a loss of linearity is observed from 700 nm onwards. Similar behaviour was observed for coatings sprayed at 900 °C. Contact stiffness linearity was observed for coatings deposited at 50, 60, and 70 bar; however, at 40 bar, non-linear behaviour was observed from 500 nm onwards. For coatings deposited at 1000 °C, the pressures of 50, 60, and 70 bar show a linear trend. However, for 40 bar, a loss of linearity occurs beginning at 600 nm of penetration. For a spray temperature of 1100 °C, the coatings showed linearity up to 400 nm of penetration depth for all coatings.

This loss of linearity observed in several coatings may be due to defects present in the microstructure of the coatings such as porosity, lack of continuity or cracking. According to the microstructure observed in previous research [31], coatings deposited at a pressure of 40 bar showed a lack of cohesion between splats combined with significant porosity. Therefore, the evolutions of the elastic moduli have been restricted only to the range of penetration depths for which the contact stiffness showed a linear trend. Fig. 5 shows the elastic modulus evolution for each coating calculated from the contact stiffness data corresponding to the linear range (Fig. 4) after applying the Oliver-Pharr method [29]. The elastic modulus values remained constant with the penetration depth in this linear range considered.

To determine the elastic-plastic behaviour of the materials, nanoindentation test were performed using two spherical indenters. Tests with a tip radius of 5 μm were used to determine the plastic branch, and tests with a tip radius of 500 μm were used to obtain the elastic branch. The development of the stress-strain curves was carried out in accordance with the equations determined by Pathak et al. [30]. The results are presented in Fig. 6. In the corresponding stress-strain curves, two zones can be distinguished. The left zone, for strain values below 0.03, represents the elastic behaviour of the material. The right zone, for higher strains, depicts the plastic one.

The region with the lower indentation strain, obtained through indentations made with a 500 μm radius indenter, is characterised by a linear trend. The slope allowed for the determination of the elastic modulus (E) by applying Hooke's law and assuming isotropic, homogeneous, and linear elastic behaviour for the material. The elastic modulus obtained for the substrates was 198 ± 28 GPa for S355J2 and 170 ± 12 GPa for SS316L. The values obtained by both indenters for the substrates have been reported by previous works [41–45]. Beghini et al. [46] proposed a finite element simulation method to deduce the stress-strain curves; these authors performed the study on SS316L, obtaining an elastic modulus of 180 ± 4 GPa. This made it possible to validate the method of obtaining the curves by spherical indentations, as well as the equations used to determine the stress-strain curves.

Fig. 7 presents a comparison of the elastic moduli obtained by both indenters for each coating. It was observed that the higher the spraying pressure, the higher the elastic modulus. However, this trend is not significant if the corresponding standard deviations are considered. In

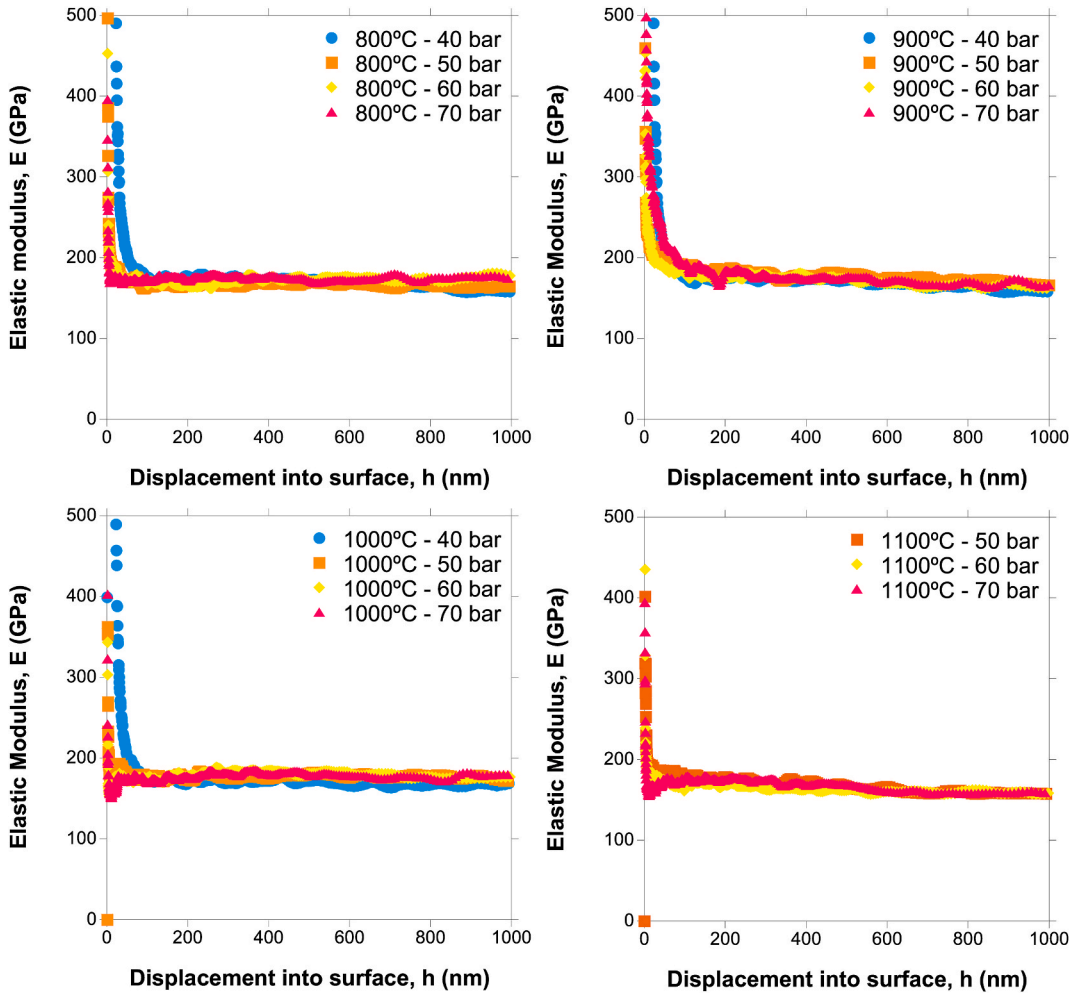

Fig. 5. Evolution of the elastic modulus versus displacement into surface for the coatings. A representative curve for each coating is presented.

the case of a Berkovich tip, eliminating the effect of porosity and other defects in the estimation of the elastic modulus becomes more difficult when they are present in higher proportions. This is attempted with the restriction of calculating the elastic modulus from contact stiffness data that show a linear trend with penetration depth. However, when the presence of defects is greater, ensuring that all contact stiffness data meet this condition is more difficult. This could happen with the data analysis of the coatings deposited at the lower spraying pressures, where the presence of defects may be higher (Fig. 1). Additionally, the elastic modulus values determined from the elastic region of the indentation stress-strain curves agree with previous studies reported by other researchers [46]. Sundararajan et al. [47] determined the elastic moduli of several CS coatings to demonstrate the usefulness of this property in quantifying the extent of inter-splat cracking. They programmed nanoindentation tests on Cu, Ag, Zn, Ta, Nb, Ti, and 316L stainless steel coatings using a Berkovich tip and applying the Oliver-Pharr method [29] on the force-displacement data. They reported a value of 193 GPa for the elastic modulus of SS 316L coatings. Additionally, Cortés et al. [28] compared the performance of 316L coatings processed by CS with those deposited by HVOF onto S355-J2 structural steel. They deposited 316L coatings at 900 °C and 50, 60, or 70 bar. In their work, the mechanical response of the coatings was measured by nanoindentation tests. They obtained elastic modulus values of 165 GPa, 175 GPa, and 185 GPa for the coatings deposited at 50, 60, and 70 bar, respectively. This study revealed the influence of porosity on the elastic modulus, indicating that the lower the porosity, the higher the elastic modulus.

The purpose of erosion tests is to evaluate the resistance of the material to wear by successive impacts of abrasive particles on its surface. In the methodology section, the erosion rate was defined as the ratio between the removed material mass and the mass of abrasive incident particles, according to Equation (6). Fig. 8 shows the erosion rates for all coatings and substrates. The coatings showed a similar or even better erosion resistance than the substrates. Only coatings sprayed at 1100 °C had worse resistance. Considering the coatings, no significant effect of the spraying pressure and temperature on the wear rates was observed. However, the coatings deposited at 1100 °C showed the highest erosion rates, even greater than those obtained on the substrates. This may be due to the activation of other mechanisms during the erosion process. In fact, the appearance of cracks was reported in previous research [27], acting as a synergistic process. The hardened microstructure of these coatings showed a lower deformation capacity, which could facilitate the appearance of this new erosion mechanism.

Fig. 9 shows representative cross sections of the residual eroded imprints of the coatings deposited at 800 °C, 900 °C, 1000 °C, and 1100 °C at 60 bar. The erosion process has never reached the substrate. Consequently, the erosion rates were not affected by the substrates. When comparing the cross sections of the eroded coatings, the one sprayed at 1100 °C showed the highest depth and width of the residual imprints. Additionally, the surface contour of the residual imprint was characterised by the presence of subsurface cracks, revealing the activation of an additional mechanism to that of plastic deformation, governed by a cracking phenomenon favoured by the lower deformation capacity of these coatings. This could justify the higher erosion rate observed after the erosion test, as referenced above.

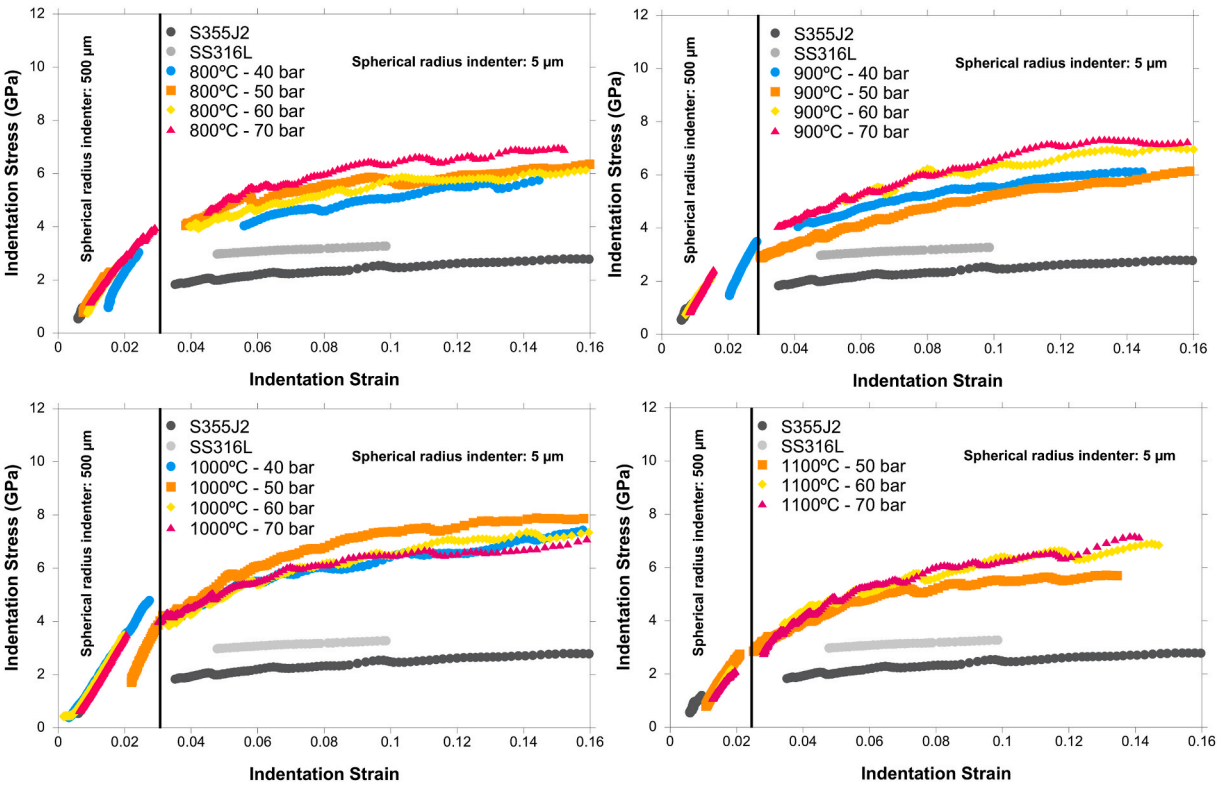

Fig. 6. Stress-strain indentation curves test representative for the different projection conditions in addition to the n addition to substrate S355J2 and substrate SS316L.

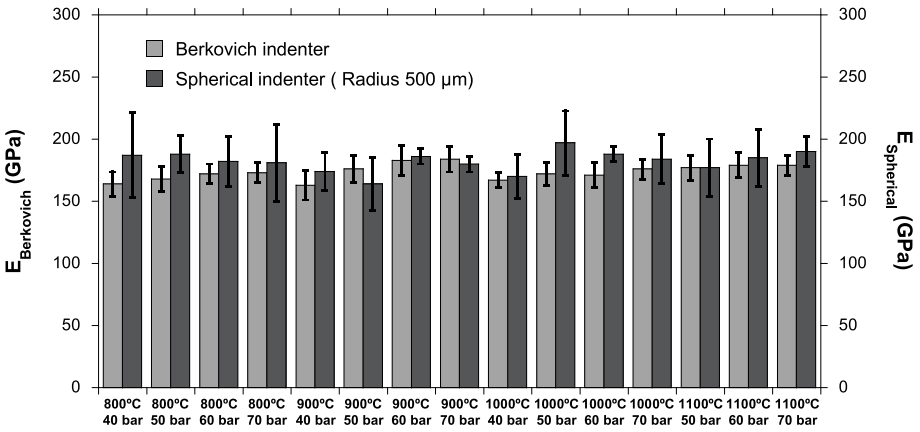

Fig. 7. Comparison of elastic modulus values of the coatings obtained from indentation tests with Berkovich and spherical tips.

Fig. 10 shows representative details of the surfaces of the eroded residual imprints obtained on the coatings deposited at 800 °C, 900 °C, 1000 °C, and 1100 °C at 60 bar. These surfaces were characterised by severe plastic deformation revealed by a controlling ploughing phenomenon; this behaviour is characteristic for ductile materials [23,35,48]. According to Hutching's studies, this is the mechanism that controls the erosion process at normal incidence on ductile materials [24].

The erosion behaviour of the coatings may be conditioned by their mechanical properties and therefore by their stress-strain curves. Parameters associated with the mechanical response of the materials have been incorporated into different predictive erosion models. The erosion model proposed by Hutchings [24] includes the critical strain and the hardness of the material (Equation (1)). Additionally, the erosion model presented by Chen et al. [49] depends on the flow stress of the material. These mechanical properties are related to the corresponding stress-strain curve of the material. Consequently, the stress-strain curve of a coating could be used, and an energy model of the erosion process could be proposed. Given that the erosion process implies a plastic deformation, in this work, the plastic branch of the corresponding stress-strain curve has been considered when proposing an energy analysis of the erosion process on the 316L coatings sprayed by CS.

First, the concept of erosion energy, $\Sigma_{erosion}$, is defined as the energy that must be accumulated in the material for the erosion process to occur. This energy is accumulated through the successive impacts of erosive particles. The energy accumulated in the material to produce the elimination of a volume element, dV, is given by the following equation:

$$d\Sigma_{erosion} = \sigma \, d\varepsilon \, dV \tag{7}$$

Consequently, the mass of material removed because of the erosion process is the mass of material that has previously stored the energy

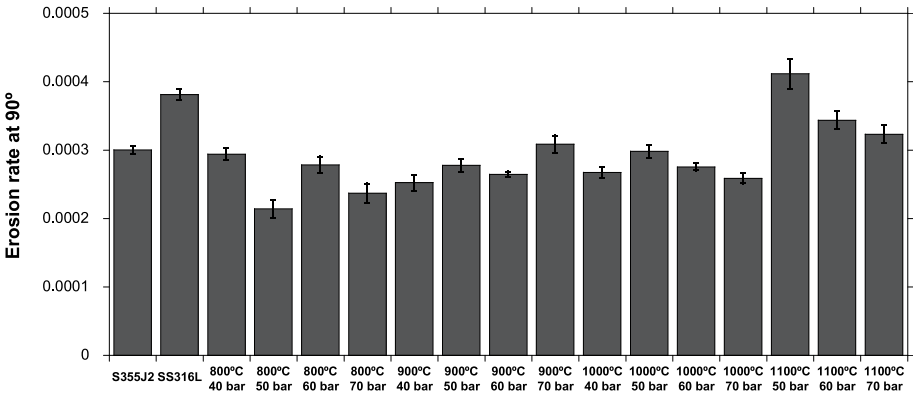

Fig. 8. Erosion rate values by different spraying conditions and substrates.

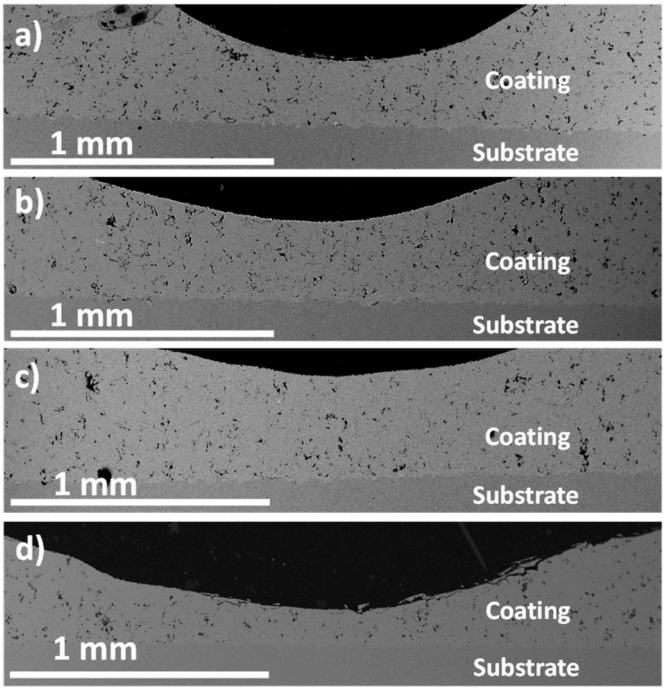

Fig. 9. Cross sections of the erosion tracks at 60 bar with different temperatures: a) 800 °C, b) 900 °C, c) 1000 °C and d) 1100 °C.

necessary for it. The total erosion energy, $\Sigma_{erosion}$, can then be expressed as:

$$\Sigma_{erosion} = \iint \sigma \, d\varepsilon \, dV = \int_0^{\varepsilon_c} \sigma \, d\varepsilon \int_0^{removed\ mass} \frac{dm}{\rho} \tag{8}$$

where, ε_c refers to the critical strain, defined in Equation (1). The first integral represents the area under the stress-strain curve of the plastic branch up to a maximum strain set by ε_c. The second integral represents the volume of material removed by erosion, expressed as a function of mass. To determine this erosion energy, the value of the ε_c should have be previously estimated. Some researchers have indicated that for ductile materials, this critical strain is around 15 % [50,51]. Therefore, the area under the stress-strain curve, Λ, is calculated for a strain interval between 5 and 15 %, and the erosion energy is given by:

$$\Sigma_{erosion} = \Lambda\,|_{\varepsilon_c=0.05-0.15} \bullet \frac{removed\ mass}{\rho} \tag{9}$$

The material is eroded because of the continuous damage induced by the impact of the erosive particles. They impact the surface of the material with a certain kinetic energy. Consequently, the amount of energy available to produce erosion is a fraction of the total kinetic energy transferred by the particles that reach the surface of the material. Therefore, this kinetic energy can be obtained according to the following equation:

$$\Sigma_{incident} = \frac{1}{2} \bullet mass\ of\ erosive\ particles \bullet v_p^2 \tag{10}$$

where v_p refers to the incident particle velocity.

Both energies can be related through an energy threshold ratio for the erosion process, η, defined as the fraction of energy required to activate the erosion process. Considering this definition and the expression of the erosion rate according to Equation (6), it is possible to define this ratio through the following relationship:

$$\eta = \frac{\Sigma_{erosion}}{\Sigma_{incident}} = \frac{2 \bullet \Lambda\,|_{\varepsilon_c=0.05-0.15}}{\rho \bullet v_p^2} \bullet T_{erosion} \tag{11}$$

The possible values for this ratio range from 0 to 1. When this parameter is 0, the total incident energy produces erosion. However, if the value is 1, no erosion occurs. Therefore, this parameter is related to the severity of the erosion process. The lower the value of this parameter, the higher the erosion rates.

The erosion model proposed by Hutchings [24] is applicable when the experimental tests are carried out at normal incidence. In such cases, the dominant erosion mechanism is ploughing controlled by plastic deformation developed by the material [34,52,53]. Accordingly, material removal takes place when the material reaches a threshold value of the strain, ε_c. Therefore, this erosion model includes a plastic behaviour criterion. Then, if the erosion model proposed by Hutchings [24] is considered, the activating threshold ratio of the erosion process, η, could give an energetic meaning to the K_D parameter (Equation (1)). To corroborate this assumption, it is necessary to calculate values of the K_D parameter for the coatings analysed in this work. Values of K_D have been obtained from the erosion rates of the coatings (Fig. 8) while considering the hardness values previously reported [27] and setting a value for the critical strain of 15 %.

Fig. 11 shows a comparison between η and K_D. The η values for the substrates and coatings were small, ranging between 0.003 and 0.009, so the energy needed to activate the erosion process was also small, revealing a high severity of the erosion process. The η values for the coatings were higher than the ones obtained for the substrates. Consequently, the energy dissipated by the volume of plastically strained material for the substrates was lower than that exhibited by the coatings. This could be explained by the hardened microstructure formed in the coatings though the CS process. Additionally, it seems that this ratio was not affected by the spraying parameters. However, the values observed for coatings deposited at 1100 °C were significantly higher. A similar tendency was observed for the K_D parameter.

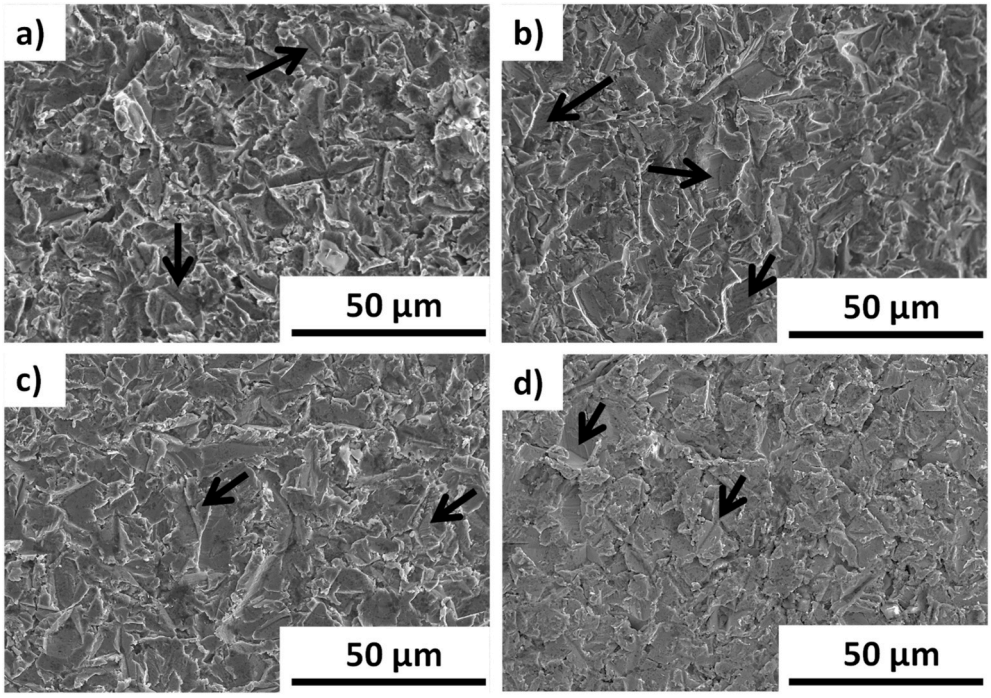

Fig. 10. Representative details of the surface of the eroded residual imprints at 60 bar with different temperatures: a) 800 °C, b) 900 °C, c) 1000 °C and d) 1100 °C.

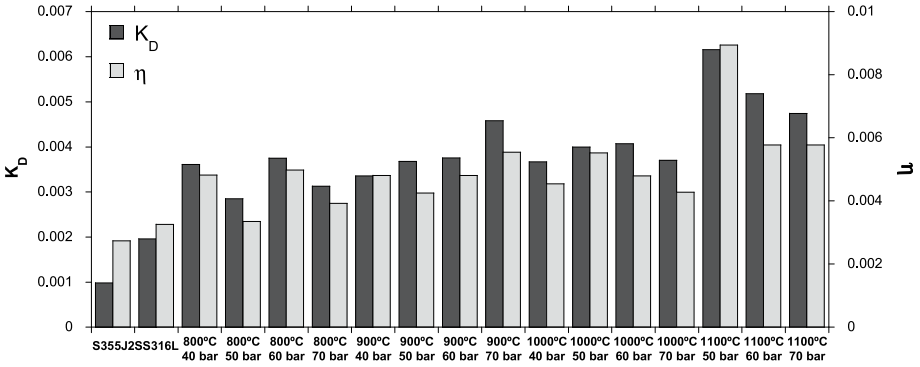

Fig. 11. Values of K_D parameter and the efficiency of the erosion process for the substrates and the different coatings.

Comparing the η values with the erosion rates (Figs. 8 and 11), the substrates showed lower η values and higher erosion rates than those showed by the coatings. However, the coatings sprayed at 1100 °C showed higher values of this ratio and higher erosion rates. Therefore, the lower the η value, the higher the wear rate and. consequently, the severity of the erosion process. The anomalous behaviour shown by the coatings deposited at 1100 °C could be due to another additional phenomenon, such as the generation of cracks, which could act as a synergistic process to damage by erosion. This circumstance was previously pointed out by Cortés et al. [27].

4. Conclusions

316L stainless steel coatings were deposited onto S355J2 carbon steel substrates to improve their resistance to erosion. Different spraying temperatures, 800 °C, 900 °C, 1000 °C and 1100 °C, combined with different pressures of the carrier gas, 40, 50, 60, and 70 bar, were analysed. The erosion rates of the coatings were determined and an energy threshold ratio was proposed to evaluate the severity of the erosion process. This work yielded the following conclusions.

- Regarding the morphology analysis of the coatings' microstructure, the thicknesses of the coatings did not show a clear correlation with the spraying conditions. The coatings sprayed at 800 °C are those with the highest values. However, they are the coatings with the greatest porosity. Nevertheless, when the coatings were sprayed at 900 °C and 1000 °C, an effect of the spray pressure was observed so that the higher the pressure, the lower the porosity. The existence of a relationship between porosity and spraying conditions is desirable from the point of view of coating manufacturing. Since this relationship is more pronounced when spraying at 1000 °C, this temperature was revealed as the ideal one to generate 316L coatings by cold spraying. Furthermore, higher thicknesses were obtained for pressures of 50 and 60 bar. However, coatings deposited at 50 bar exhibited higher porosity. Consequently, 60 bar was revealed as the optimal pressure to spray 316L coatings by CS.
- Regarding the elastic modulus, the values obtained by both indenters, Berkovich and spherical, were similar, and no tendency with respect to the spraying parameters was observed. Consequently, the coatings are constituted by the same phases, regardless of the spraying conditions. This condition is characteristic of the CS process.

- Considering the erosion behaviour, the coatings showed similar or even lower erosion rates than the substrates. The coatings presented similar erosion rates, with no significant effect of spraying conditions, and the dominant wear mechanism was plastic deformation. Only coatings sprayed at 1100 °C had worse erosion resistance, probably due to the activation of an additional mechanism aligned with the propagation of cracks. This result discards the condition of 1100 °C for the spraying of 316L coatings by CS.
- Additionally, the mechanical response of the coatings was included in the erosion behaviour of the coatings through an energetic balance. An energy threshold ratio was proposed that allows for discriminating the severity of the erosion process. This coefficient revealed the significantly poor erosion behaviour of the coatings deposited at 1100 °C of spraying temperature. This circumstance allowed for this temperature of coating deposition to be ruled out from the point of view of erosion.

CRediT authorship contribution statement

Rocío Cortés: Writing – review & editing, Validation, Methodology, Investigation, Formal analysis, Conceptualization. **Miguel Ángel Garrido-Maneiro:** Formal analysis, Conceptualization, Investigation, Methodology, Validation, Writing – original draft, Writing – review & editing. **Pedro Poza:** Writing – review & editing, Writing – original draft, Supervision, Methodology, Conceptualization.

Declaration of competing interest

The authors declare the following financial interests/personal relationships which may be considered as potential competing interests:

Pedro Poza reports financial support was provided by Ministry of Science Technology and Innovations. If there are other authors, they declare that they have no known competing financial interests or personal relationships that could have appeared to influence the work reported in this paper.

Data availability

No data was used for the research described in the article.

Acknowledgements

The authors would like to acknowledge the financial support received from the Spanish government, CICYT, under grants MAT2016-76928-C2-2-R (DURESPRAY) and Agencia Estatal de Investigación PID2020- 115508RB-C22 (A3M).

References

[1] T. Schmidt, F. Gärtner, H. Assadi, H. Kreye, Development of a generalized parameter window for cold spray deposition, Acta Mater. 54 (2006) 729–742, https://doi.org/10.1016/J.ACTAMAT.2005.10.005.
[2] P. Poza, M.Á. Garrido-Maneiro, Cold-sprayed coatings: microstructure, mechanical properties, and wear behaviour, Prog. Mater. Sci. 123 (2022), https://doi.org/10.1016/j.pmatsci.2021.100839.
[3] J. Karthikeyan, The advantages and disadvantages of the cold spray coating process, The Cold Spray Materials Deposition Process: Fundamentals and Applications (2007) 62–71, https://doi.org/10.1533/9781845693787.1.62.
[4] R.N. Raoelison, C. Verdy, H. Liao, Cold gas dynamic spray additive manufacturing today: deposit possibilities, technological solutions and viable applications, Mater. Des. 133 (2017) 266–287, https://doi.org/10.1016/J.MATDES.2017.07.067.
[5] M. Grujicic, J.R. Saylor, D.E. Beasley, W.S. DeRosset, D. Helfritch, Computational analysis of the interfacial bonding between feed-powder particles and the substrate in the cold-gas dynamic-spray process, Appl. Surf. Sci. 219 (2003) 211–227, https://doi.org/10.1016/S0169-4332(03)00643-3.
[6] G. Bae, S. Kumar, S. Yoon, K. Kang, H. Na, H.J. Kim, C. Lee, Bonding features and associated mechanisms in kinetic sprayed titanium coatings, Acta Mater. 57 (2009) 5654–5666, https://doi.org/10.1016/J.ACTAMAT.2009.07.061.
[7] A. Moridi, S.M. Hassani-Gangaraj, M. Guagliano, A hybrid approach to determine critical and erosion velocities in the cold spray process, Appl. Surf. Sci. 273 (2013) 617–624, https://doi.org/10.1016/J.APSUSC.2013.02.089.
[8] T. Schmidt, H. Assadi, F. Gärtner, H. Richter, T. Stoltenhoff, H. Kreye, T. Klassen, From particle acceleration to impact and bonding in cold spraying, J. Therm. Spray Technol. 18 (2009) 794–808, https://doi.org/10.1007/s11666-009-9357-7.
[9] T. Stoltenhoff, H. Kreye, H.J. Richter, An analysis of the cold spray process and its coatings, J. Therm. Spray Technol. 11 (2002) 542–550, https://doi.org/10.1361/105996302770348682, 2002 11:4.
[10] W. Li, C. Huang, M. Yu, H. Liao, Investigation on mechanical property of annealed copper particles and cold sprayed copper coating by a micro-indentation testing, Mater. Des. 46 (2013) 219–226, https://doi.org/10.1016/J.MATDES.2012.10.029.
[11] W.Y. Li, H. Liao, G. Douchy, C. Coddet, Optimal design of a cold spray nozzle by numerical analysis of particle velocity and experimental validation with 316L stainless steel powder, Mater. Des. 28 (2007) 2129–2137, https://doi.org/10.1016/j.matdes.2006.05.016.
[12] Y. Li, X. Wang, S. Yin, S. Xu, Influence of particle Initial temperature on high velocity impact process in cold spraying, Procedia Environ Sci 12 (2012) 298–304, https://doi.org/10.1016/J.PROENV.2012.01.281.
[13] L. Alonso, M.A. Garrido, P. Poza, An optimisation method for the cold-spray process: on the nozzle geometry, Mater. Des. 214 (2022) 110387, https://doi.org/10.1016/j.matdes.2022.110387.
[14] Z. Shabani Chafjiri, A. Abdollah-zadeh, R.A. Seraj, A. Azarniya, Effect of cold spray processing parameters on the microstructure, wear, and corrosion behavior of Cu and Cu–Al2O3 coatings deposited on AZ31 alloy substrate, Results in Engineering 20 (2023) 101594, https://doi.org/10.1016/J.RINENG.2023.101594.
[15] M. Villa, S. Dosta, J.M. Guilemany, Optimization of 316L stainless steel coatings on light alloys using Cold Gas Spray, Surf. Coat. Technol. 235 (2013) 220–225, https://doi.org/10.1016/j.surfcoat.2013.07.036.
[16] C. Xue, Research on steel structure technology in civil engineering construction, IOP Conf. Ser. Earth Environ. Sci. 474 (2020), https://doi.org/10.1088/1755-1315/474/7/072072.
[17] K.F. Amin, H.M.M.A. Rashed, Steel used in construction industries, Reference Module in Materials Science and Materials Engineering (2019), https://doi.org/10.1016/B978-0-12-803581-8.10270-X.
[18] I.M. Chohan, A. Ahmad, N. Sallih, N. Bheel, M. Ali, A.F. Deifalla, A review on life cycle assessment of different pipeline materials, Results in Engineering 19 (2023) 101325, https://doi.org/10.1016/J.RINENG.2023.101325.
[19] A.M. El-Sherik, Trends in oil and gas corrosion research and Technologies. http://www.sciencedirect.com:5070/book/9780081011058/trends-in-oil-and-gas-corrosion-research-and-technologies, 2017. (Accessed 4 December 2023).
[20] J. Bień, K. Jakubowski, T. Kamiński, J. Kmita, P. Kmita, P.J.S. Cruz, M. Maksymowicz, Railway bridge defects and degradation mechanisms. https://repositorium.sdum.uminho.pt/handle/1822/9132, 2007. (Accessed 4 December 2023).
[21] C.A. Widener, O.C. Ozdemir, M. Carter, Structural repair using cold spray technology for enhanced sustainability of high value assets, Procedia Manuf. 21 (2018) 361–368, https://doi.org/10.1016/J.PROMFG.2018.02.132.
[22] M.A. Islam, T. Alam, Z.N. Farhat, A. Mohamed, A. Alfantazi Effect of microstructure on the erosion behavior of carbon steel, (n.d.). https://doi.org/10.1016/j.wear.2014.12.004.
[23] M.A. Chowdhury, N. Hossain, M. Shahin, U.K. Debnath, M. Rahman, M. M. Rahman, Erosion characteristics of stainless steels under different percentage of SiC- Al2O3-Fe2O3 solid particles, Tribol. Int. 167 (2022) 107403, https://doi.org/10.1016/J.TRIBOINT.2021.107403.
[24] I.M. Hutchings, A model for the erosion of metals by spherical particles at normal incidence, Wear 70 (1981) 269–281, https://doi.org/10.1016/0043-1648(81)90347-1.
[25] A.A. Hussain, S.B. Wesley, H.S. Goyal, A.P. Harsha, Investigations on Solid Particle Erosion Behaviour of Ferritic Steels, Austenitic Steel and Low Carbon Steel and Correlation of Erosion Data with Erosion Model, vol. 227, Institution of Mechanical Engineers, 2012, pp. 234–245, https://doi.org/10.1177/1350650112459128.
[26] S. Singh, J. Singh Grewal, K. Rakha, Erosion wear performance of HVOF and cold spray coatings deposited on T-91 boiler steel, Mater Today Proc 62 (2022) 7509–7516, https://doi.org/10.1016/J.MATPR.2022.04.277.
[27] R. Cortés, M.Á. Garrido-Maneiro, P. Poza, Evaluating the effect of deposition conditions on the local wear resistance of cold sprayed stainless steel coatings, Wear 530–531 (2023) 205066, https://doi.org/10.1016/J.WEAR.2023.205066.
[28] R. Cortés, M.A. Garrido, A. Rico, C.J. Múnez, P. Poza, A.M. Martos, S. Dosta, I. G. Cano, Effect of processing conditions on the mechanical performance of stainless steel cold sprayed coatings, Surf. Coat. Technol. 394 (2020) 125874, https://doi.org/10.1016/j.surfcoat.2020.125874.
[29] W.C. Oliver, G.M. Pharr, An improved technique for determining hardness and elastic modulus using load and displacement sensing indentation experiments, J. Mater. Res. 7 (1992) 1564–1583, https://doi.org/10.1557/JMR.1992.1564.
[30] S. Pathak, S.R. Kalidindi, Spherical nanoindentation stress–strain curves, Mater. Sci. Eng. R Rep. 91 (2015) 1–36, https://doi.org/10.1016/J.MSER.2015.02.001.
[31] R. Cortés, M.Á. Garrido, P. Poza, A. Martos, S. Dosta, I. García, Cold sprayed coatings for repairing damaged metallic structures, Key Eng. Mater. 813 (2019) 74–79, https://doi.org/10.4028/WWW.SCIENTIFIC.NET/KEM.813.74.
[32] A.C. Fischer-Cripps, Nanoindentation, 2004, p. 263.
[33] ASTM G76 - 18 Standard Test Method for Conducting Erosion Tests by Solid Particle Impingement Using Gas Jets, (n.d.) https://www.astm.org/Standards/G76 (accessed November 3, 2021).
[34] S. Tortuero, M.A. Garrido, P. Poza, J. Rodríguez, Evaluating the erosion resistance of Ti6Al4V coatings deposited by cold spray, Wear 454–455 (2020) 203337, https://doi.org/10.1016/J.WEAR.2020.203337.

[35] V.B. Nguyen, Q.B. Nguyen, Y.W. Zhang, C.Y.H. Lim, B.C. Khoo, Effect of particle size on erosion characteristics, Wear 348–349 (2016) 126–137, https://doi.org/10.1016/J.WEAR.2015.12.003.
[36] J. Huang, W. Ma, Y. Xie, H. Fukanum, K. Zhang, G. Wang, R. Huang, Influence of cold gas spray processing conditions on the properties of 316L stainless steel coatings, Surf. Eng. 35 (2019) 784–791, https://doi.org/10.1080/02670844.2019.1584967.
[37] S. Adachi, N. Ueda, Effect of cold-spray conditions using a nitrogen propellant gas on AISI 316L stainless steel-coating microstructures, Coatings 7 (2017), https://doi.org/10.3390/coatings7070087.
[38] P. Coddet, C. Verdy, C. Coddet, F. Debray, F. Lecouturier, Mechanical properties of thick 304L stainless steel deposits processed by He cold spray, Surf. Coat. Technol. 277 (2015) 74–80, https://doi.org/10.1016/J.SURFCOAT.2015.07.001.
[39] J.B. Yan, Y. Geng, P. Xie, J. Xie, Low-temperature mechanical properties of stainless steel 316L: tests and constitutive models, Constr Build Mater 343 (2022) 128122, https://doi.org/10.1016/J.CONBUILDMAT.2022.128122.
[40] B. Bhushan, Depth-sensing nanoindentation measurement techniques and applications, Microsyst. Technol. 23 (2017) 1595–1649, https://doi.org/10.1007/S00542-017-3372-2, 2017 23:5.
[41] V. Milovanović, D. Arsić, M. Milutinović, M. Živković, M. Topalović, A comparison study of fatigue behavior of S355J2+N, S690QL and X37CrMoV5-1 steel, Metals 12 (2022) 1199, https://doi.org/10.3390/MET12071199, 2022, Vol. 12, Page 1199.
[42] T.-lęzak, L.-niezek, A comparative LCF study of S960QL high strength steel and S355J2 Mild steel, Procedia Eng. 114 (2015) 78–85, https://doi.org/10.1016/J.PROENG.2015.08.044.
[43] C.T. Lachowicz, R. Owsiński, Comparative analysis of fatigue energy characteristics of S355J2 steel subjected to Multi-Axis Loads, Materials 13 (2020) 2470, https://doi.org/10.3390/MA13112470, 2020, Vol. 13, Page 2470.
[44] W. Macek, Z. Marciniak, R. Branco, D. Rozumek, G.M. Królczyk, A fractographic study exploring the fracture surface topography of S355J2 steel after pseudo-random bending-torsion fatigue tests, Measurement 178 (2021) 109443, https://doi.org/10.1016/J.MEASUREMENT.2021.109443.
[45] K.A. Mohammad, E.S. Zainudin, S. Sapuan, N.I. Zahari, A. Ali, Fatigue life for type 316L stainless steel under cyclic loading, Adv Mat Res 701 (2013) 77–81, https://doi.org/10.4028/WWW.SCIENTIFIC.NET/AMR.701.77.
[46] M. Beghini, L. Bertini, V. Fontanari, Evaluation of the stress–strain curve of metallic materials by spherical indentation, Int J Solids Struct 43 (2006) 2441–2459, https://doi.org/10.1016/J.IJSOLSTR.2005.06.068.
[47] G. Sundararajan, N.M. Chavan, S. Kumar, The elastic modulus of cold spray coatings: influence of inter-splat boundary cracking, J. Therm. Spray Technol. 22 (2013) 1348–1357, https://doi.org/10.1007/S11666-013-0034-5/TABLES/5.
[48] J.R. Laguna-Camacho, M. Vite-Torres, E.A. Gallardo-Hernández, E.E. Vera-Cárdenas, Solid particle erosion on different metallic materials, Tribology in Engineering (2013), https://doi.org/10.5772/51176.
[49] D. Chen, M. Sarumi, S.T.S. Al-Hassani, S. Gan, Z. Yin, A model for erosion at normal impact, Wear 205 (1997) 32–39, https://doi.org/10.1016/S0043-1648(96)07315-2.
[50] D. Cruz, M.A. Garrido, C.J. Múnez, A. Rico, P. Poza, Erosion of cold sprayed aeronautical coatings* 35 (2019) 792–800, https://doi.org/10.1080/02670844.2019.1586096, 1586096.
[51] B.F. Levin, K.S. Vecchio, J.N. DuPont, A.R. Marder, Modeling solid-particle erosion of ductile alloys, Metall. Mater. Trans. 30 (1999) 1763–1774, https://doi.org/10.1007/S11661-999-0175-9, 1999 30:7.
[52] S. Ahmad Alidokht, P. Vo, S. Yue, R.R. Chromik, Erosive wear behavior of Cold-Sprayed Ni-WC composite coating, Wear 376–377 (2017) 566–577, https://doi.org/10.1016/J.WEAR.2017.01.052.
[53] A. Mishra, C.K. Behera, S. Mohan, A. Mohan, Erosive wear of 446SS ferritic steel: a potential material for heat exchangers application, Mater. Res. Express 5 (2018) 106522, https://doi.org/10.1088/2053-1591/aadb55.